Supporting Information for

Photoactivated Covalent Metal-Organic Frameworks with Dual Functionalities for efficient Colorimetric Sensing and Aerobic Oxidation Reaction

Jiani Yang,[1] Chao Xiong,[1] Mi Zhou,[1] Xianglin Luo,[1] Xikui Liu, [1] Chong Cheng,[1] Chao He,[1,] and Xiaohui Xu[1,2]**

[1] Department of Medical Ultrasound, College of Polymer Science and Engineering, National Key Laboratory of Advanced Polymer Materials, West China Hospital, Sichuan University, Chengdu 610041, China

[2] Frontiers Science Center for Disease-Related Molecular Network, West China Hospital, Sichuan University, Chengdu 610041, China

* Corresponding to: hec918@scu.edu.cn (C. He) and xiaohuixu@scu.edu.cn (X. Xu)

Experimental Sections

1. Synthesis of Ag_3L_3 metal clusters

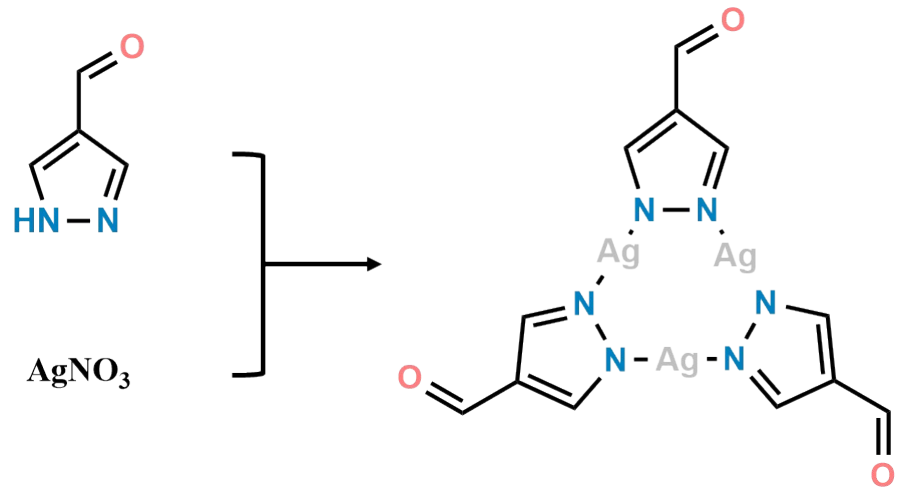

Ag_3L_3 was synthesized according to previously reported procedures[1]. A mixture of the ligand 1H-pyrazole-4-carbaldehyde (HL) (96 mg, 1.0 mmol), $AgNO_3$ (170 mg, 1.0 mmol), 30 mL acetonitrile, and 0.4 mL triethylamine was added into a 50 mL glass bottle. Then, the resulting mixture was stirred for 4 hours in the dark. Afterward, the resulting residue was washed with acetonitrile and absolute ethanol and filtered to give white powders (218.92 mg, yield:82.3%).

2. Synthesis of Cu_3L_3 metal clusters

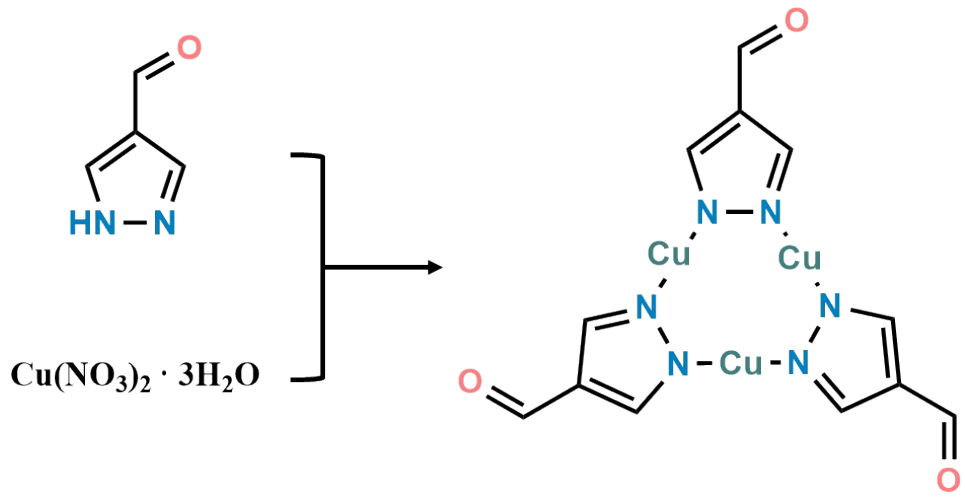

Cu_3L_3 was synthesized according to previously reported procedures[2]. $Cu(NO_3)_2 \cdot 3H_2O$ (200 mg, 0.83

mmol) and HL (96 mg, 1.0 mmol) were dissolved in a mixture of 6.7 mL DMF, 5.0 mL H_2O, and 6.7 mL ethanol in a 25 mL vial. The tightly capped vial was placed in an oven at 100 ℃ for 12 h, and light yellow single crystals were obtained. The crystals were collected and immersed in H_2O for 3 days, during which time H_2O was exchanged three times per day. Afterward, the crystals were quickly washed with acetone three times, followed by drying under vacuum at 120 ℃ for 24 h (230.58 mg, yield:77.9%).

3. Stability Test

CMOFs were immersed in NaOAc-HOAc buffer (pH = 4), DMF, EtOH, THF and acetonitrile (ACN) for 12 h, respectively. The mixture was then filtered and washed with methanol and dried under vacuum at 60 °C. Then, the PXRD patterns were collected.

4. Photoelectrochemical measurements

All the electrochemical measurements were carried out in a conventional three-electrode cell using the Gamry reference 600 workstations (Gamry, USA) at room temperature. Mott Schottky, photocurrent, and Electrochemical Impedance Spectroscopy (EIS) were tested in Na_2SO_4 solution (0.5 M, pH 7). The working electrode is an Indium-Tin Oxide (ITO) glass plate coated with catalyst slurry; the counter electrode is platinum foil, and saturated Ag/AgCl is the reference electrode. Mott Schottky plots were measured at alternating current (AC) frequencies of 500 Hz, 1000 Hz, and 1500 Hz. Working electrode preparation: 10 mg of catalyst, 1 mL of ethanol, and 10 μL of Nafion were mixed and sonicated for 20 min. 50 μL of slurry was deposited evenly on the ITO glass plate (1 ×1 cm^2), which was dried under infrared irradiation.

5. Oxidase-like activity of Tbpa-Ag_3 and Tbpa-Cu_3 under darkness or light irradiation

The catalytic activity of two CMOFs was evaluated by catalytic oxidation of TMB. Typically, under darkness, 20 μL of Tbpa-Ag_3 or Tbpa-Cu_3 (10 mg mL^{-1}) was added firstly into 1955 μL of 0.2 M HAc-NaAc buffer solution (pH 4.0), containing 25 μL of TMB (10 mg·mL^{-1} in DMSO). Then, the test was started quickly at room temperature. After the 5 min incubation at 25 °C, the oxidase-like activity was measured by monitoring the absorbance at 652 nm for the oxTMB after centrifugation. Oxidase-like activity of Tbpa-Ag_3 and Tbpa-Cu_3 was measured under the same conditions as above, with the only difference being that the incubation was performed under a Xenon lamp (λ≥420 nm, 100 mW/cm^2).

6. Steady-state enzyme dynamic parameters

The Michaelis-Menten constant was calculated based on the Michaelis-Menten saturation curve. For each TMB or H_2O_2 concentration, the initial reaction rates (V_0) were calculated from the absorbance variation using the Beer-Lambert Law (Equation (1)). The reaction rates were then plotted against their corresponding TMB concentration and then fitted with the Michaelis–Menten curves (Equation (2)). Furthermore, a linear double-reciprocal plot (Lineweaver–Burk plot, Equation (3)) was used to determine the maximum reaction velocity (V_{max}) and Michaelis constant (K_m).

$$A = \varepsilon lc \quad (1)$$

Where, ε is 39,000 M^{-1} cm^{-1} for oxTMB, c indicates the oxTMB concentration, and l is the length of the solution in the light path.

$$V_0 = \frac{V_{max} * [S]}{K_m + [S]} \quad (2)$$

$$\frac{1}{V_0} = \frac{K_m}{V_{max}} \cdot \frac{1}{[S]} + \frac{1}{V_{max}} \quad (3)$$

Where, [S] is the concentration of TMB.

7. Colorimetric detection of L-Cys and GSH

For the sensing procedure, 20 μL of Tbpa-Ag_3 (10 mg mL^{-1}) was added firstly into 1955 μL of 0.2 M HAc-NaAc buffer solution (pH 4.0), containing 25 μL of TMB (10 mg·mL^{-1} in DMSO) and different amounts of L-Cys or GSH. After the 5 min incubation under light irradiation (λ≥420 nm, 100 mW/cm^2), the supernatant was collected by centrifugation, and 200 μL of the supernatant was added to the 96-well plate, and the absorption at 652 nm was recorded in a microplate reader. To investigate the selectivity of this systems, water, NaCl, Na_2SO_4, KCl, and some common amino acids were chosen as the interfering substances.

8. Catalytic coupling reactions of benzylamines and their derivatives

5 mg CMOFs powder, 0.2 μM benzylamine or its derivatives, 0.2 μM chlorine benzene (internal standard), and 2 mL acetonitrile were added to the quartz glass tube. The glass tube was sealed with a rubber stopper and oxygen bubbling was carried out for 10 minutes. Subsequently, glass tube was placed under blue light (460 nm) illumination for 4 hours. After the reaction was completed, the filtrate was collected and detected by GC and NMR. When conducting the quenching experiment, quenching agents were added additionally to explore the active species in the catalytic process.

Supplementary Figures

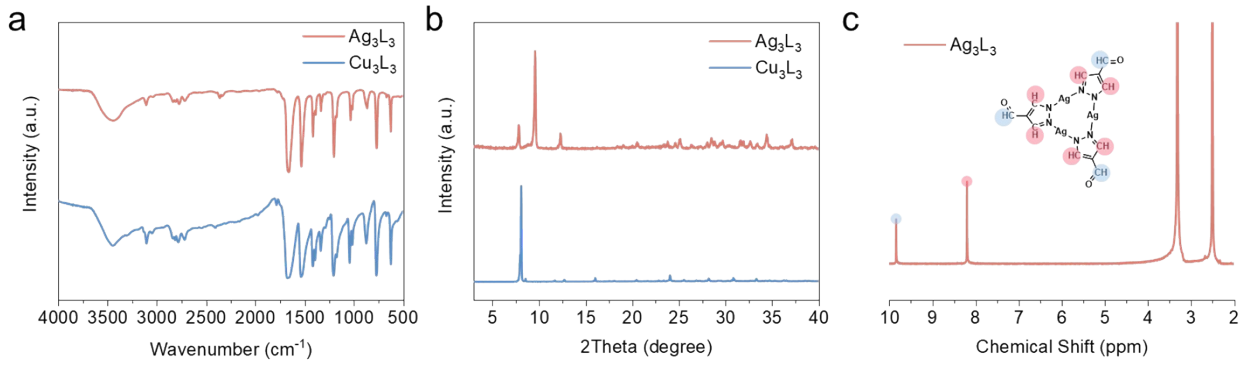

Fig. S1. (a) FT-IR spectra, (b) PXRD patterns and (c) ^{1}H-NMR spectrum of Ag_3L_3 and Cu_3L_3.

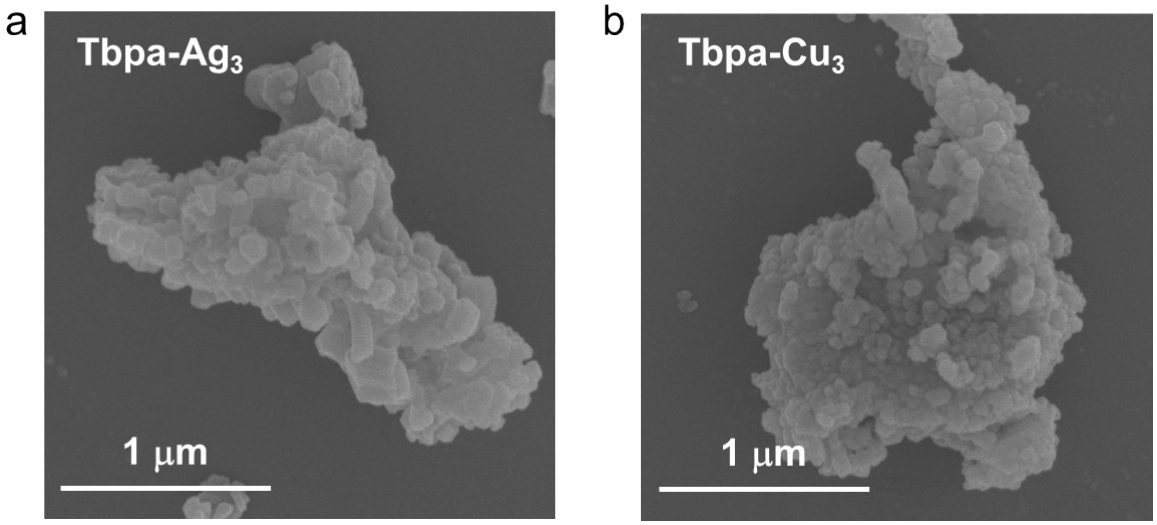

Fig. S2. SEM images of (a) Tbpa-Ag_3 and (b) Tbpa-Cu_3.

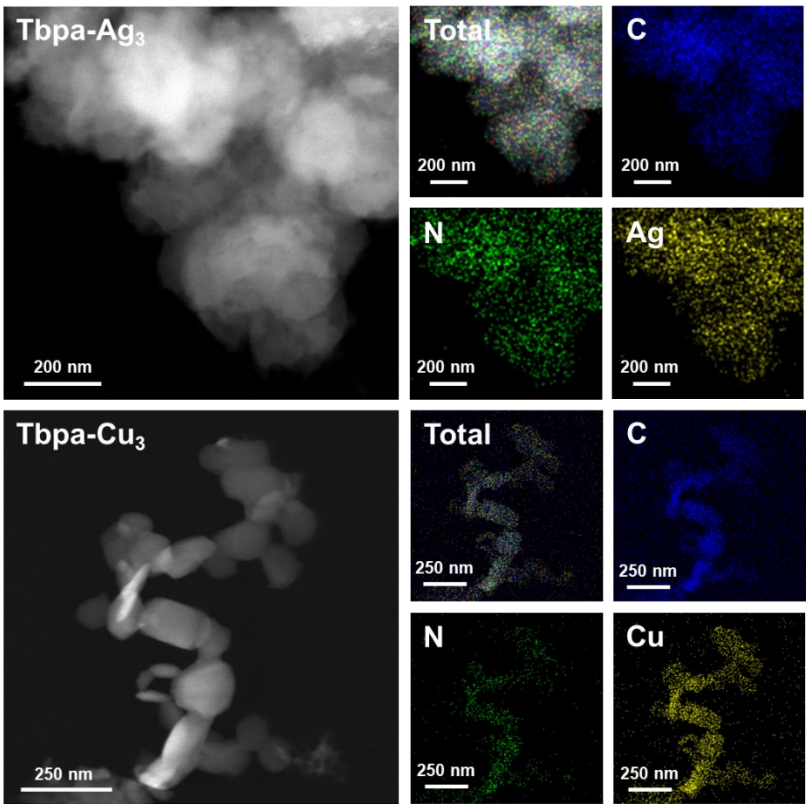

Fig. S3. The energy-dispersive X-ray spectroscopy (EDX) mapping images of Tbpa-Ag_3 and Tbpa-Cu_3.

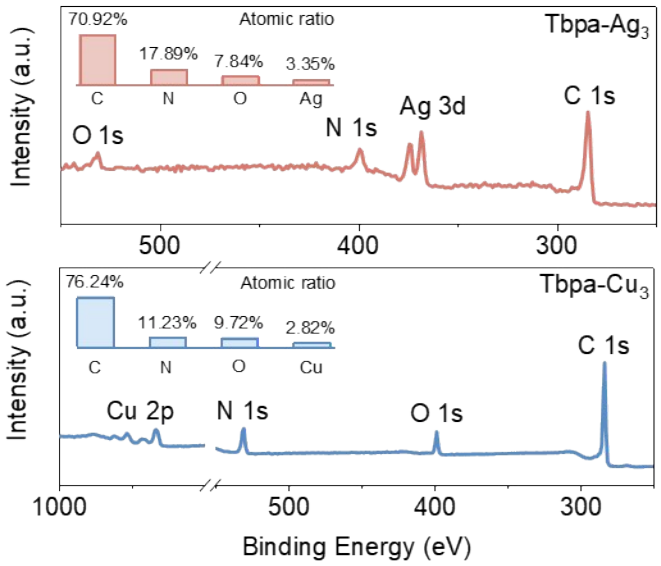

Fig. S4. The survey XPS spectrum of two CMOFs.

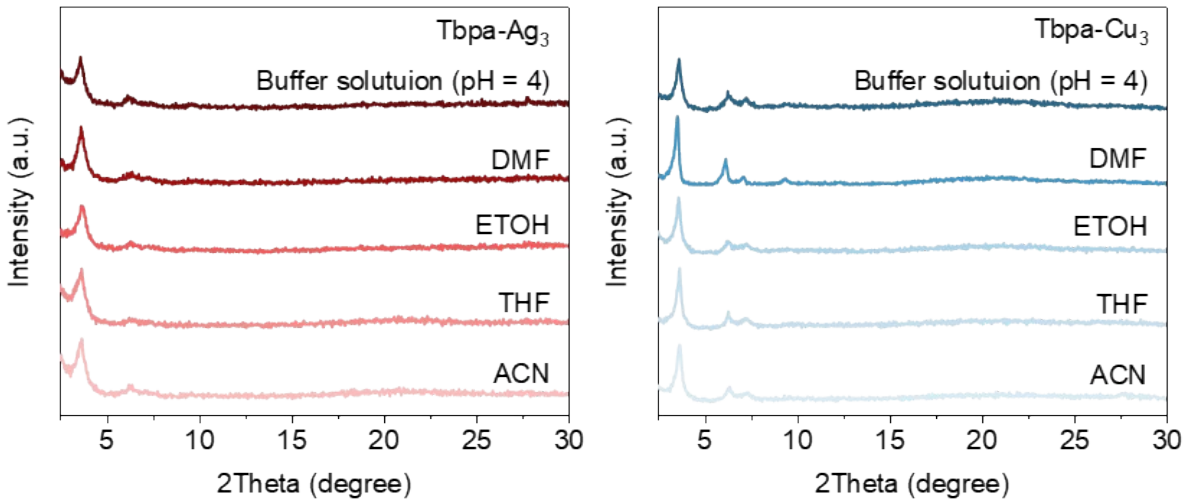

Fig. S5. PXRD patterns of the (a) Tbpa-Ag_3 and (b) Tbpa-Cu_3 upon 12 h treatment in different conditions.

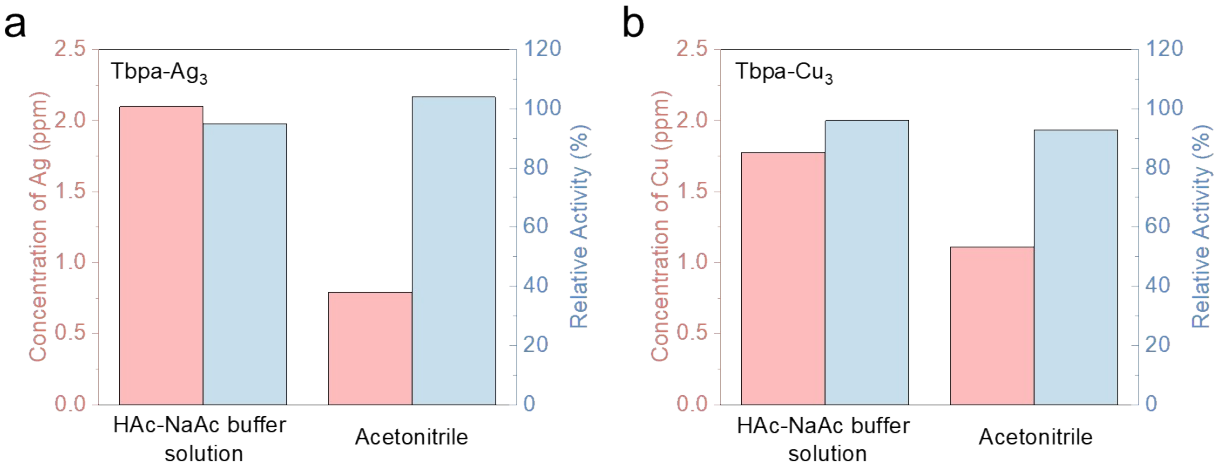

Fig. S6. The ionic leaching concentrations of two CMOFs in solution and their relative activities after soaking.

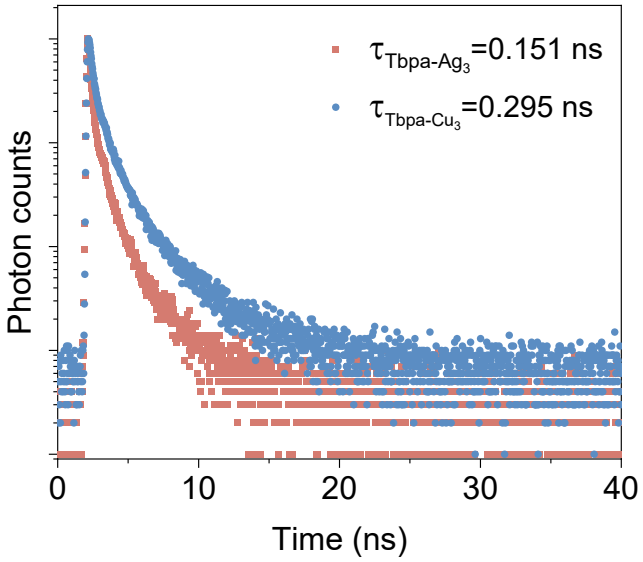

Fig. S7. Time-resolved PL spectra of Tbpa-Ag_3 and Tbpa-Cu_3.

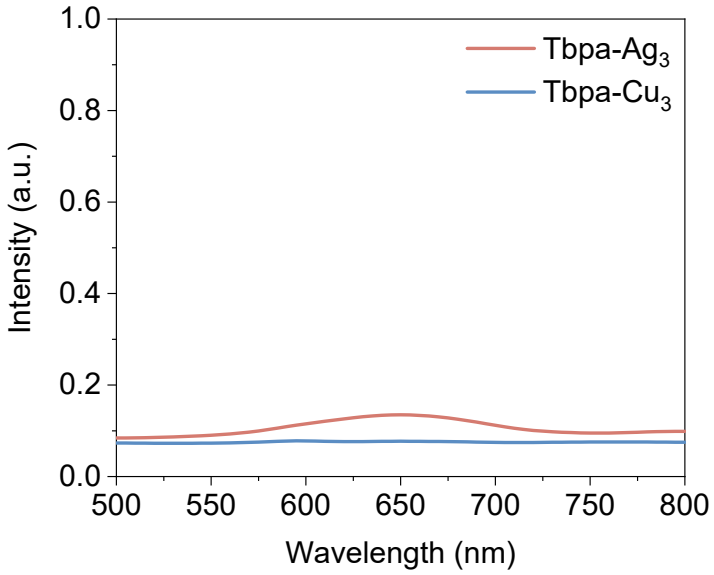

Fig. S8. UV-vis absorption spectra of the OXD-like performances for Tbpa-Ag_3 and Tbpa-Cu_3 under darkness.

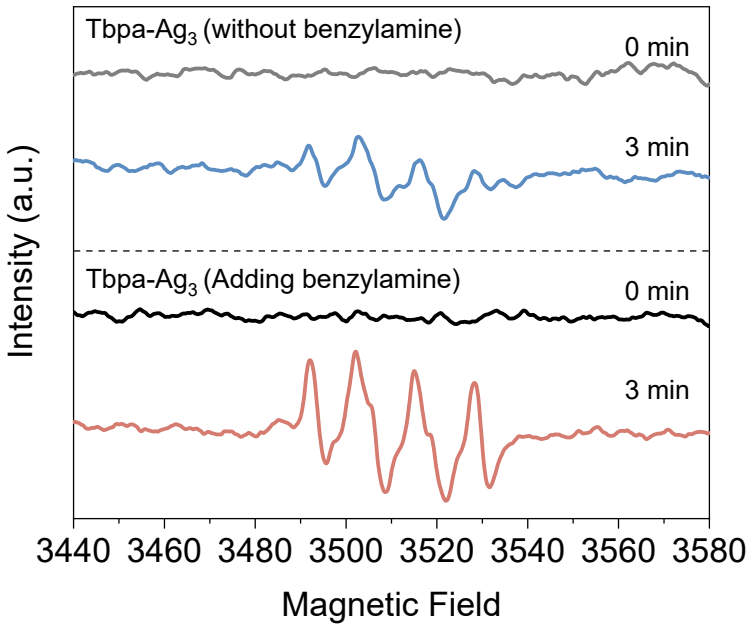

Fig. S9. EPR spectra of Tbpa-Ag_3 under different reaction conditions.

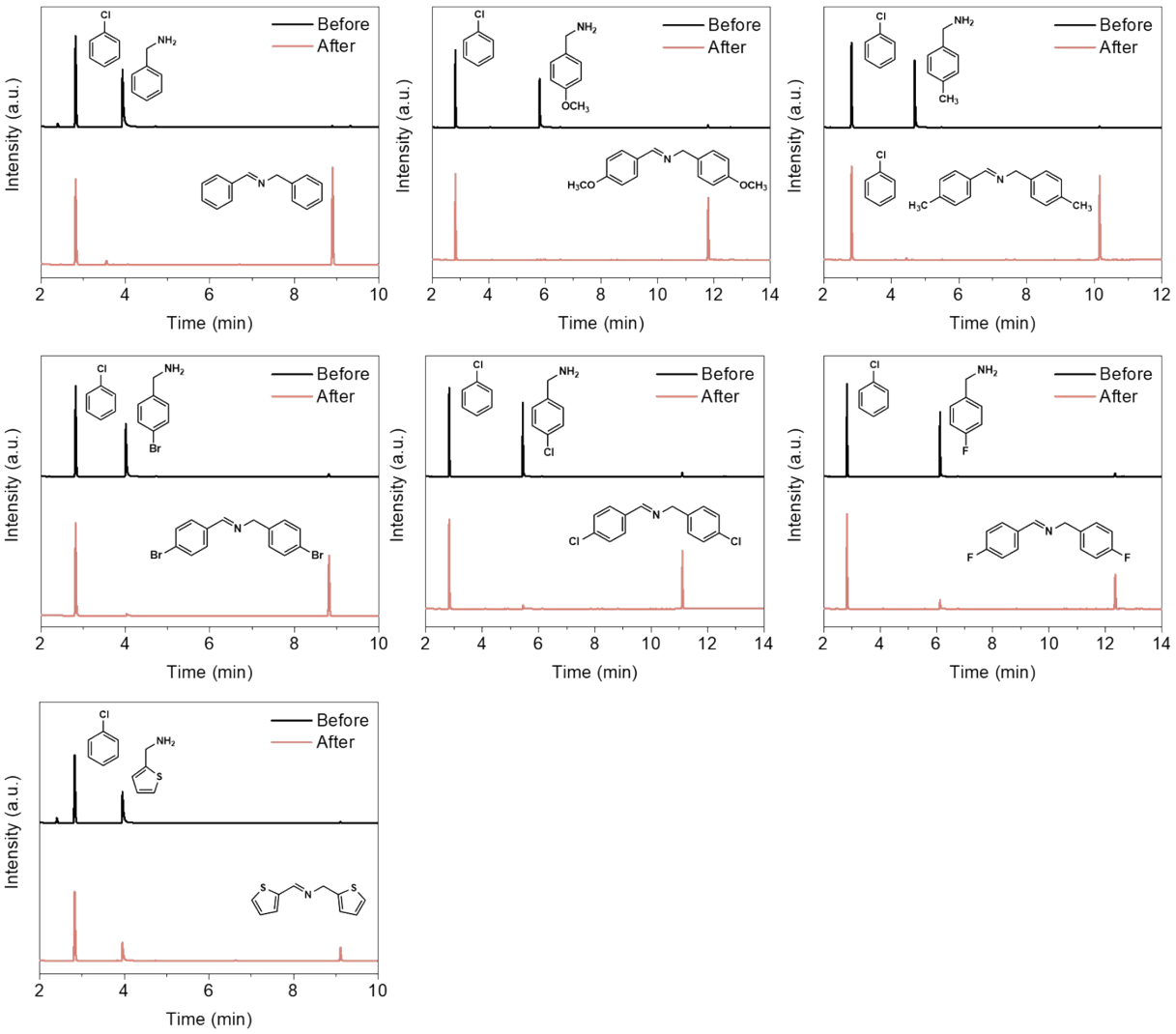

Fig. S10. GC data for different substrates before and after catalysis.

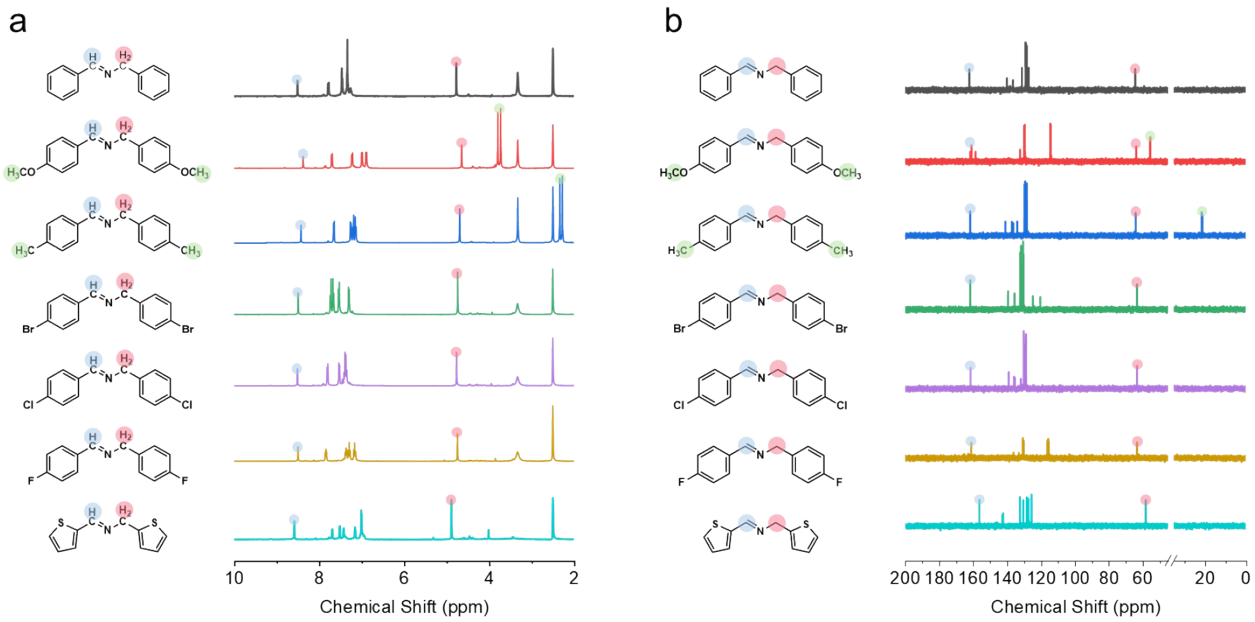

Fig. S11. ^{1}H-NMR and ^{13}C-NMR spectra for different substrates after catalysis.

Table S1. The structure model of Tbpa-Ag_3 with *P3* mode.

Tbpa-Ag_3 Space group: Trigonal *P3* $a = b = 28.8283$ Å, $c = 3.5564$ Å $\alpha = 90.0°$, $\beta = 90.0°$, $\gamma = 120.0°$			
Atom	x	y	z
C1	1.49889	-0.00458	-0.0056
C2	1.55218	0.02363	-0.09121
C3	1.57946	0.07839	-0.08761
C4	1.55377	0.10599	0.00304
C5	1.50045	0.07781	0.09269
C6	1.47323	0.02303	0.09063
C7	1.58254	0.164	0.00514
C8	1.63227	0.19202	0.15629
C9	1.65911	0.24675	0.16037
C10	1.63798	0.27566	0.00722
C11	1.58801	0.24655	-0.14661
C12	1.5605	0.19181	-0.14461
N13	1.47298	-0.06086	-0.0112
C14	1.48447	0.57731	-0.00724
C15	1.44843	0.59803	-0.01003
C16	1.46199	0.65022	-0.01077
N17	1.41758	0.65258	-0.0121
N18	1.37691	0.60446	-0.01218
C19	1.3942	0.56999	-0.01095
Ag20	1.30464	0.58992	-0.01239
H21	1.57255	0.003	-0.16377
H22	1.62046	0.0992	-0.16033

Table S2. The structure model of Tbpa-Cu_3 with *P3* mode.

Tbpa-Cu_3 Space group: Trigonal *P3* $a = b = 28.9304$ Å, $c = 3.2208$ Å $\alpha = 90.0°$, $\beta = 90.0°$, $\gamma = 120.0°$			
Atom	x	y	z
C1	1.4989	-0.00456	-0.00549
C2	1.55218	0.02363	-0.09125
C3	1.57946	0.07839	-0.08801
C4	1.55378	0.106	0.00241
C5	1.50047	0.07785	0.09217
C6	1.47325	0.02306	0.09049
C7	1.58255	0.16402	0.00426
C8	1.63227	0.19204	0.15544
C9	1.65912	0.24677	0.15936
C10	1.63799	0.27567	0.00609
C11	1.58804	0.24656	-0.14776
C12	1.56054	0.19182	-0.14567
N13	1.47299	-0.06084	-0.0106
C14	1.48448	0.5773	-0.00635
C15	1.44844	0.59802	-0.0086
C16	1.46199	0.65022	-0.00906
N17	1.41758	0.65258	-0.00993
N18	1.37691	0.60445	-0.01
C19	1.3942	0.56998	-0.00922
Cu20	1.30464	0.58991	-0.00993
H21	1.57254	0.00299	-0.16361
H22	1.62045	0.09919	-0.16078

Table S3. Comparison of the OXD-like catalytic kinetic constants with other reported biocatalysts.

Biocatalyst	Substrate	K_m (mM)	V_{max} (M s^{-1})	Ref
Fe-N-C	TMB	1.81	6.0×10^{-9}	[3]
Mn-UMOF	TMB	0.42	3.0×10^{-8}	[4]
Fluorescein	TMB	0.16	6.7×10^{-8}	[5]
CeO_2	TMB	0.42	1.0×10^{-7}	[6]
MnOOH	TMB	1.00	3.3×10^{-7}	[7]
Pd_{12}	TMB	0.24	7.1×10^{-8}	[8]
Tbpa-Ag_3	TMB	0.07	2.42×10^{-7}	This work
Tbpa-Cu_3	TMB	0.11	1.24×10^{-7}	This work

Table S4. Comparison of the OXD-like catalytic kinetic constants with other reported photo-responsive biocatalysts.

Biocatalyst	Substrate	K_m (mM)	V_{max} (M s^{-1})	Ref
Py-TT COF	TMB	0.04	5.26×10^{-8}	[9]
ETTA-Tz COF	TMB	0.22	1.8×10^{-7}	[10]
COF-300-AR	TMB	0.09	3.38×10^{-8}	[11]
TTPA-COF	TMB	0.09	2.4×10^{-7}	[12]
COF-Por-DPP	TMB	0.198	4.52×10^{-8}	[13]
TpBTD	TMB	0.10	1.8×10^{-7}	[14]
Tbpa-Ag_3	TMB	0.07	2.42×10^{-7}	This work
Tbpa-Cu_3	TMB	0.11	1.24×10^{-7}	This work

Table S5. Performance comparison of Tbpa-Ag_3 with earlier reported biocatalysts in the detection of L-Cys.

Biocatalysts	Linear range (μM)	LOD (μM)	Ref.
Au@NH_2-MIL-125	1-10	0.15	[15]
Co-N/C-900	1-40	0.033	[16]
Ru@V_2O_4	3-50	0.139	[17]
$NiCo_2O_4$	2-40	0.3	[18]
PrOx-NR	0.2-10	0.0003	[19]
Tbpa-Ag_3	4-80	0.27	This work

Table S6. Performance comparison of Tbpa-Ag_3 with earlier reported biocatalysts in the detection of GSH.

Biocatalysts	Linear range (μM)	LOD (μM)	Ref.
MnPNP	0.05-10	0.022	[20]
Co,N-HPC	0.05-30	0.036	[21]
Mn_3O_4	5-60	0.889	[22]
MnO_2	1-25	0.3	[23]
TiO_2/C-QDs	0.5-25	0.2	[24]
Tbpa-Ag_3	4-70	0.19	This work

References

1. Y.-Y. Tang, X. Luo, R.-Q. Xia, J. Luo, S.-K. Peng, Z.-N. Liu, Q. Gao, M. Xie, R.-J. Wei, G.-H. Ning and D. Li, *Angewandte Chemie International Edition*, 2024, **63**, e202408186.
2. R.-J. Wei, H.-G. Zhou, Z.-Y. Zhang, G.-H. Ning and D. Li, *CCS Chemistry*, 2020, **3**, 2045-2053.
3. Y. Wu, L. Jiao, X. Luo, W. Xu, X. Wei, H. Wang, H. Yan, W. Gu, B. Z. Xu, D. Du, Y. Lin and C. Zhu, *Small*, 2019, **15**, 1903108.
4. A. K. Singh, K. Bijalwan, N. Kaushal, A. Kumari, A. Saha and A. Indra, *ACS Applied Nano Materials*, 2023, **6**, 8036-8045.
5. L. Liu, C. Sun, J. Yang, Y. Shi, Y. Long and H. Zheng, *Chemistry - A European Journal*, 2018, **24**, 6148-6154.
6. H. Cheng, S. Lin, F. Muhammad, Y.-W. Lin and H. Wei, *ACS Sensors*, 2016, **1**, 1336-1343.
7. L. Yu, H. Li, W. Huang, H. Yu and Y. He, *Inorganic Chemistry*, 2021, **60**, 5264-5270.
8. S. Bhattacharyya, S. R. Ali, M. Venkateswarulu, P. Howlader, E. Zangrando, M. De and P. S. Mukherjee, *Journal of the American Chemical Society*, 2020, **142**, 18981-18989.
9. G. Li, W. Ma, Y. Yang, C. Zhong, H. Huang, D. Ouyang, Y. He, W. Tian, J. Lin and Z. Lin, *ACS Applied Materials & Interfaces*, 2021, **13**,

49482-49489.

10. G. Li, W. Tian, C. Zhong, Y. Yang and Z. Lin, *ACS Applied Materials & Interfaces*, 2022, **14**, 21750-21757.
11. P. Jin, X. Niu, F. Zhang, K. Dong, H. Dai, H. Zhang, W. Wang, H. Chen and X. Chen, *ACS Applied Materials & Interfaces*, 2020, **12**, 20414-20422.
12. Y. Peng, M. Huang, L. Chen, C. Gong, N. Li, Y. Huang and C. Cheng, *Nano Research*, 2022, **15**, 8783-8790.
13. W. Yao, L. Yao, Z.-E. Wang, X. Song and Z. Liang, *Talanta*, 2025, **286**, 127519.
14. L. Liang, Y. Jiang, F. Liu, J. Wu, L. Tian, S. Zhao and F. Ye, *Sensors and Actuators B: Chemical*, 2023, **381**, 133422.
15. Y. Zhang, J. Song, W. Shao and J. Li, *Microporous and Mesoporous Materials*, 2021, **310**, 110642.
16. J. Chen, S. Hu, Y. Cai, X. Liu, Y. Wu, Y. Dai and Z. Wang, *Analyst*, 2022, **147**, 915-922.
17. J. Hou, P. Jia, K. Yang, T. Bu, X. Sun and L. Wang, *Sensors and Actuators B: Chemical*, 2021, **344**, 130266.
18. S.-W. Lv, N. Zhao, J.-M. Liu, F.-E. Yang, C.-Y. Li and S. Wang, *ACS Applied Materials & Interfaces*, 2021, **13**, 25044-25052.
19. L. Jiang, Y. Han, S. Fernández-García, M. Tinoco, Z. Li, P. Nan, J. Sun, J. J. Delgado, H. Pan, G. Blanco, J. Martínez-López, A. B. Hungría, J. J. Calvino and X. Chen, *Applied Surface Science*, 2023, **610**, 155502.
20. N. K. Dega, A. B. Ganganboina, H. L. Tran, E. P. Kuncoro and R.-a. Doong, *Talanta*, 2022, **237**, 122957.
21. S. Li, L. Wang, X. Zhang, H. Chai and Y. Huang, *Sensors and Actuators B: Chemical*, 2018, **264**, 312-319.
22. J. Xi, C. Zhu, Y. Wang, Q. Zhang and L. Fan, *RSC Advances*, 2019, **9**, 16509-16514.
23. J. Liu, L. Meng, Z. Fei, P. J. Dyson, X. Jing and X. Liu, *Biosensors and Bioelectronics*, 2017, **90**, 69-74.
24. Z. Jin, G. Xu, Y. Niu, X. Ding, Y. Han, W. Kong, Y. Fang, H. Niu and Y. Xu, *Journal of Materials Chemistry B*, 2020, **8**, 3513-3518.